animal and vegetal poles. Presumably, this shift reflects the reorganization of cytoskeletal components after the egg is fertilized (*30*). As a consequence, Cdx2 mRNA and presumably other transcripts associated with components of the cytoskeleton (*31*) can then be distributed unequally between the two blastomeres when the zygote divides.

The asymmetry in *Cdx2* mRNA distribution observed in oocytes persisted in embryo stages: one-cell (23 of 32), two-cell (25 of 33), four-cell (26 of 36), and eight-cell (30 of 38) (Fig. 5, D to O), although it remains unclear whether the transcripts are entirely of maternal origin or newly transcribed from the embryonic genome. In most instances, the asymmetry was remarkable, with half the blastomeres showing little evidence for the presence of *Cdx2* transcripts. The relatively homogeneous distribution of *Eomes* mRNA in control oocytes and embryos indicated that the asymmetry of *Cdx2* was not an artifact (fig. S9). At the blastocyst stage, *Cdx2* mRNA was confined to trophectoderm and absent from the ICM (21 of 28) (Fig. 5, S to U). The signal in blastocysts, although outside the nuclei, was generally highly concentrated. We have no explanation for this phenomenon, although it might relate to fixation or permeability artifacts. We confirmed the asymmetric distribution of *Cdx2* transcripts in two- and four-cell embryos by performing reverse transcription polymerase chain reaction (RT-PCR) on RNA from individual blastomeres dissected from embryos (Fig. 5V) and likewise proved that *Cdx2* mRNA was present in metaphase II oocytes. Together, these data show that the localization of *Cdx2* mRNA in the oocyte accurately predicts the lineage of cells destined for trophectoderm.

One puzzle is why $Cdx2^{-/-}$ embryos have been reported to form temporary (*24*) or even complete (*25*) blastocoel cavities, whereas our studies indicate that knock-down of *Cdx2* mRNA in the lagging blastomere of two-cell-stage embryos leads to complete trophectoderm failure. The most likely explanation is that sufficient maternal oocyte *Cdx2* mRNA persists in $Cdx2^{-/-}$ embryos to define the trophectoderm lineage but not to ensure its eventual ability to function.

Our data are at odds with the mainstream view that blastomeres of two-, four- and eight-cell mouse embryos are essentially equivalent (*14*–*16*). Instead, they support the opposing view that individual blastomeres of early embryos can have dissimilar fates (*17*–*23*).

References and Notes

1. C. Nusslein-Volhard, *Dev. Suppl.* **1**, 1 (1991).
2. M. L. King, T. J. Messitt, K. L. Mowry, *Biol. Cell.* **97**, 19 (2005).
3. A. K. Tarkowski, *Nature* **184**, 1286 (1959).
4. A. K. Tarkowski, *Nature* **190**, 857 (1961).
5. J. Rossant, *J. Embryol. Exp. Morphol.* **36**, 283 (1976).
6. S. M. Willadsen, *J. Embryol. Exp. Morphol.* **65**, 165 (1981).
7. C. A. Ziomek, M. H. Johnson, A. H. Handyside, *J. Exp. Zool.* **221**, 345 (1982).
8. W. H. Johnson *et al.*, *Vet. Rec.* **137**, 15 (1995).
9. A. K. Tarkowski, W. Ozdzenski, R. Czolowska, *Int. J. Dev. Biol.* **45**, 811 (2001).
10. G. Schatten, P. Donovan, *Nature* **430**, 301 (2004).
11. G. Vogel, *Science* **308**, 782 (2005).
12. J. Rossant, P. P. Tam, *Dev. Cell* **7**, 155 (2004).
13. R. L. Gardner, T. J. Davies, *Philos. Trans. R. Soc. London Ser. B* **358**, 1331 (2003).
14. V. B. Alarcon, Y. Marikawa, *Biol. Reprod.* **69**, 1208 (2003).
15. T. Hiiragi, D. Solter, *Nature* **430**, 360 (2004).
16. N. Motosugi *et al.*, *Genes Dev.* **19**, 1081 (2005).
17. K. Piotrowska *et al.*, *Development* **128**, 3739 (2001).
18. B. Plusa *et al.*, *Nature* **434**, 391 (2005).
19. R. L. Gardner, *Development* **128**, 839 (2001).
20. K. Piotrowska-Nitsche *et al.*, *Development* **132**, 479 (2005).
21. T. Fujimori, Y. Kurotaki, J. Miyazaki, Y. Nabeshima, *Development* **130**, 5113 (2003).
22. M. Zernicka-Goetz, *Nat. Rev. Mol. Cell Biol.* **6**, 919 (2005).
23. R. L. Gardner, *Birth Defects Res. Part C* **75**, 142 (2005).
24. D. Strumpf *et al.*, *Development* **132**, 2093 (2005).
25. E. Tolkunova *et al.*, *Stem Cells* **24**, 139 (2006).
26. K. Deb, M. Sivaguru, H. Y. Yong, R. M. Roberts, unpublished data.
27. J. McConnell *et al.*, *Mol. Reprod. Dev.* **71**, 399 (2005).
28. S. Fraser, R. Keynes, A. Lumsden, *Nature* **344**, 431 (1990).
29. P. Brulet, C. Babinet, R. Kemler, F. Jacob, *Proc. Natl. Acad. Sci. U.S.A.* **77**, 4113 (1980).
30. D. Gray *et al.*, *Curr. Biol.* **14**, 397 (2004).
31. A. P. Takizawa *et al.*, *Nature* **389**, 90 (1997).

32. We thank L. Spate for technical assistance; B. Hardiman and the Molecular Cytology Core, Life Science Center, for help with confocal microscopy; and. S. Westfall and anonymous reviewers for their constructive input during preparation of the manuscript. The research was supported by NIH grants R01 HD21896 and R01 HD42201 to R.M.R. and NIH grant R01 RR13438 to R. Prather (for salary support for H.Y.Y.).

Supporting Online Material

www.sciencemag.org/cgi/content/full/311/5763/992/DC1
Materials and Methods
SOM Text
Figs. S1 to S9
References

4 October 2005; accepted 13 January 2006
10.1126/science.1120925

X-ray Structure of a Self-Compartmentalizing Sulfur Cycle Metalloenzyme

Tim Urich,[1] Cláudio M. Gomes,[2] Arnulf Kletzin,[1]* Carlos Frazão[2]*

Numerous microorganisms oxidize sulfur for energy conservation and contribute to the global biogeochemical sulfur cycle. We have determined the 1.7 angstrom–resolution structure of the sulfur oxygenase reductase from the thermoacidophilic archaeon *Acidianus ambivalens*, which catalyzes an oxygen-dependent disproportionation of elemental sulfur. Twenty-four monomers form a large hollow sphere enclosing a positively charged nanocompartment. Apolar channels provide access for linear sulfur species. A cysteine persulfide and a low-potential mononuclear non-heme iron site ligated by a 2-His-1-carboxylate facial triad in a pocket of each subunit constitute the active sites, accessible from the inside of the sphere. The iron is likely the site of both sulfur oxidation and sulfur reduction.

The microbial oxidation of reduced inorganic sulfur compounds and elemental sulfur to sulfate is one of the major reactions in the global sulfur cycle (*1*, *2*). These reactions provide the energy for the growth of many microorganisms that are essential in biotechnological processes, such as biomining of base and precious metal sulfide ores. Sulfur oxidation also plays an important role in the formation of acid mine drainage, a process that causes serious environmental problems (*3*). In addition, sulfur is among the major energy sources in the light-independent ecosystems of hydrothermal vents, solfataras, and hot springs (*4*), where chemolithoautotrophic microorganisms constitute the basis of the food chains.

Despite much research (*1*, *2*, *5*, *6*), the only example of sulfur oxidation understood at a molecular level is the oxidation of thiosulfate by the Sox complex, the prototype of sulfur compound–oxidizing enzymes isolated from the periplasm of mesophilic and neutrophilic bacteria. Here, both sulfur atoms of the substrate are oxidized to sulfate without formation of free intermediates and with c-type cytochromes as electron acceptors (*5*, *6*).

Much less is known about the oxidation of the virtually insoluble elemental sulfur (5 μg/l H_2O at 25°C) (*7*) and about sulfur-compound oxidation in acidophilic microorganisms, although these are the major players in bioleaching and acid mine drainage formation. Sulfur oxygenase reductases (SOR) are the best known examples of enzymes that oxidize elemental sulfur. They are different from other enzymes because they catalyze a distinctive oxygen-dependent sulfur disproportionation reaction with sulfite, thiosulfate, and hydrogen sulfide as products (Fig. 1C) (*8*, *9*). External cofactors

[1]Darmstadt University of Technology, Institute of Microbiology and Genetics, Schnittspahnstrasse 10, 64287 Darmstadt, Germany. [2]Universidade Nova de Lisboa, Instituto de Tecnologia Química e Biológica, Avenida da República EAN, 2781-901 Oeiras, Portugal.

*To whom correspondence should be addressed. E-mail kletzin@bio.tu-darmstadt.de (A.K.); frazao@itqb.unl.pt. (C.F.)

or electron carriers are not required. The cytoplasmic SOR has been isolated from three different thermophilic and acidophilic Archaea (fig. S1A) and catalyzes the initial step in the sulfur oxidation pathway in these organisms (*8*–*12*). The *Acidianus ambivalens* SOR is a homomultimeric thermozyme with a temperature range of 50°C to 108°C (*8*, *12*). It contains a mononuclear non-heme iron site with a reduction potential unusually low for this type of iron center (–268 mV) (*12*).

Here, we describe the x-ray structure of the recombinant *A. ambivalens* SOR and assign structural determinants for its reaction mechanism. We propose that a cysteine-bound oligomeric sulfane sulfur chain is the substrate of disproportionation and oxygenation at the iron site and, further, that dissolved and linear sulfur species are the actual substrates and not the regular α-S_8 ring.

The crystal structure of the recombinant SOR was determined by isomorphous replacement with anomalous scattering using crystals soaked with mercury and gold ions (*13*) and refined against 1.7 Å resolution native data (R/R_{free} = 18.3/21.0%) (table S1). The asymmetric unit contains six crystallographically independent SOR monomers. The holoenzyme model (Fig. 1, A and B) was generated by applying the crystallographic four-fold rotation operator of the space group I4. The SOR is a homo-oligomer composed of 24 subunits and forms a hollow sphere with pseudo-432 point-group symmetry and a calculated molecular mass of 871 kD (fig. S2, A and B, and movie S1) (*14*). The sphere has an external diameter of ~150 Å and occupies a volume of 1333 nm^3 (inner cavity included). The dimensions of the SOR oligomer are consistent with the size of the particles previously observed in electron micrographs (*8*, *12*), showing that it represents the biologically active molecule. Striking features of the oligomer's outer surface are six chimney-like protrusions composed of four-helix bundles at the four-fold symmetry axes surrounded by ring-shaped grooves (Fig. 1A and fig. S2D). No continuous channel connects the interior with the surface, because small barriers occlude these "chimneys" (fig. S2, C and D). Solely hydrophobic residues (Phe and Val) contribute to the inner chimney surface (fig. S1A). The enclosed inner compartment has a starlike shape with dimensions of ~71 to 107 Å and a volume of 347 nm^3 (fig. S2D and movie S1). Several small pockets at monomer interfaces and two wider pockets within each individual monomer are connected by narrow channels to the central compartment. Calculated electrostatics of the particle's outer surface show a positive ring surrounding the neutral entrance of the chimneys (fig. S2C). The inner surface is dominated by positive charges, mainly due to the contribution of the Fe^{III} ions (fig. S2D). The SOR's overall architecture resembles that of ferritins, which are smaller proteins displaying an identical point-group symmetry and comprising an inner cavity, which serves as an iron reservoir (*15*).

The monomers have a distorted triangular shape and are symmetrically distributed over the sphere, oriented tangential to the particle (Fig. 1B). The formation of a spherical icosatetramer

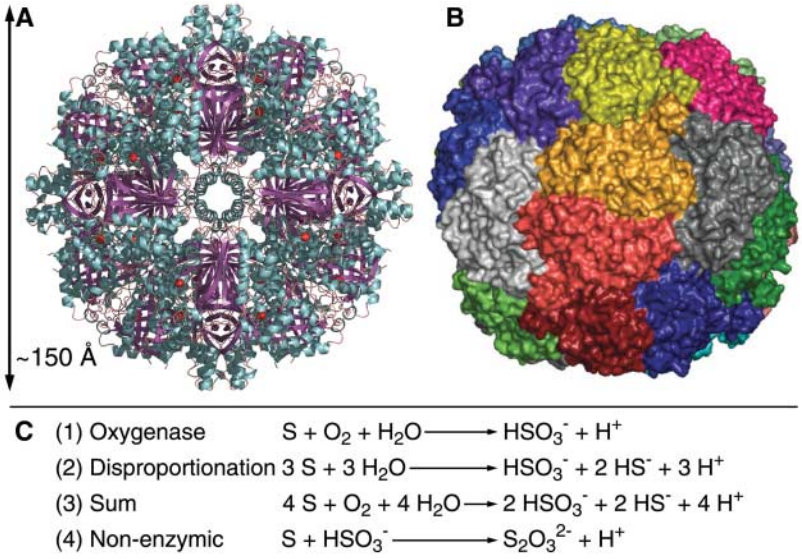

Fig. 1. The SOR holoenzyme. (**A**) Cartoon representation viewed along the crystallographic four-fold axis; α helices are colored cyan, β sheets are purple, and Fe ions are shown as red spheres. Note the protrusions at four-fold pseudosymmetry axes. (**B**) Molecular accessible surface representation with monomers colored differently and viewed along a noncrystallographic two-fold axis. Each monomer has five neighbors. (**C**) The catalytic reaction is an oxygen-dependent sulfur disproportionation with a 1:1 stoichiometry of oxidized and reduced products (Eq. 3) (*8*, *9*). Formally, it can be split into a sulfur oxygenation and a sulfur disproportionation reaction (Eqs. 1 and 2). Thiosulfate is thought to result from a nonenzymic reaction (Eq. 4) under excess S^0.

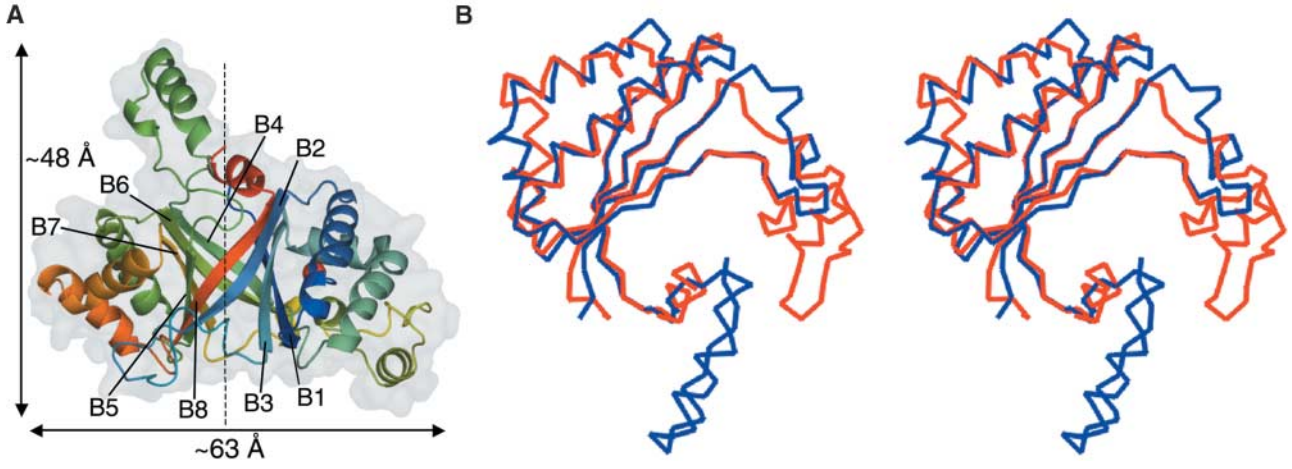

Fig. 2. The SOR monomer. (**A**) Cartoon representation showing secondary structure elements (B, β sheets) colored from blue (N-terminal) to red (C-terminal); red sphere, Fe ion; gray, the monomer's envelope; dashed line, the β barrel's two-fold pseudosymmetry axis approximately parallel to the paper plane. (**B**) Stereo view of the superposition of the two monomer halves, showing their high degree of structural similarity.

implies the formation of distinct intermediate assembly stages. We have postulated a homodimer as the basic building block of the holoenzyme from biochemical data (*12*). Analysis of the intersubunit contacts showed that two monomers share 16% of their total surface area, nearly twice as much as other monomer pairs (table S2). These monomers likely form the homodimeric building blocks (fig. S3A).

The SOR monomer is an αβ protein, formed by an internal β barrel partially surrounded by α helices (Fig. 2A and fig. S3B). The β barrel is formed by eight antiparallel β strands showing remarkable pseudosymmetry of two sets of four strands each (residues 2 to 154 and 155 to 308, respectively) (fig. S1B), related by a two-fold rotation through the barrel axis (Fig. 2A). Each half is reminiscent of the ferredoxin $(\beta\alpha\beta)_2$ topology (fig. S3, C and D) (*16*). The barrel differs from any of the three classical antiparallel β barrels (*17*), but it was recently found in two monooxygenases (Protein Data Bank entries 1lq9 and 1sqe) (*18*, *19*) and in two proteins of unknown function (1t0t and 1vdh) (*20*). Superimposing the two halves reveals a 70% overlap between C_α's to a 1.75 Å cutoff and a root mean square deviation of 1.6 Å (Fig. 2B), despite low sequence similarity in the structure-guided alignment (fig. S1B). The presence of two similar domains in one protein was first described for bovine liver rhodanese (*21*) and was later found in many protein structures (*22*), most of which show low sequence similarity between the domains. These likely result from a gene duplication and fusion event of an ancestor protein.

Three conserved cysteines (Cys31, Cys101, and Cys104 in *A. ambivalens* numbering) (fig. S1A) and a mononuclear nonheme iron site are important for catalysis (*12*, *23*, *24*). These components are located in close vicinity along a cavity within each monomer, constituting the enzyme's catalytic pocket (Fig. 3B). The minimal Fe-Fe distances are ~37 Å, which makes electronic interactions between single centers unlikely (movie S1), although possible cooperative effects cannot be excluded. The 24 catalytic pockets are deeply buried in the interior of each subunit. They are accessible exclusively from the interior of the sphere by a narrow channel from the central compartment (Fig. 3B and fig. S4A). Two methionines, Met296 and Met297 (fig. S1A) are located at the entrance of the pockets. They show flexible side chains, as judged from their alternating conformations and atomic displacement parameters, which might ease substrate access.

Each mononuclear non-heme iron center is located at the distal end of the catalytic pocket. The iron is ligated to His86, His90, and Glu114 (bidentate) (Fig. 3A). Two solvent water molecules, Wat1 and Wat2, complete a distorted octahedral coordination sphere (fig. S4B). The nature and spatial distribution of the protein ligands characterize them as a variation of the 2-His-1-carboxylate facial triad motif (*25*). The Fe ion is typically coordinated by two His and one Asp or Glu residue, constituting one face of an octahedron, with the opposite face of the coordination sphere free for the addition of exogenous ligands. Numerous metalloenzymes with nonrelated activities use this structural motif for iron binding and catalysis. Although the carboxylate ligand is monodentate in most cases, there are also examples for bidentate liganding (*25*–*27*). The protein ligands are conserved in all SOR sequences known to date (fig. S1A), as is the sequence motif H-x_3-H-x_{23}-E. Functionally, the structural similarity of the metal center with 2-His-1-carboxylate facial triad enzymes points to a mechanistic analogy, with the SOR iron center being the probable site for oxygen binding and activation. The low reduction potential, compared with other 2-His-1-carboxylate facial triad enzymes (*25*), may result from H-bonding around the Fe site. The presence of a strictly conserved acidic residue (Glu87) may also contribute to an increased stabilization, making Fe a weaker oxidant.

We and others have shown by site-directed mutagenesis that only one of the three conserved cysteine residues is essential in catalysis (Cys31) (*23*, *24*). All cysteines are located in the active site pocket at distances between 7.8 and 12.4 Å to the iron (Fig. 3B). Cys101 and

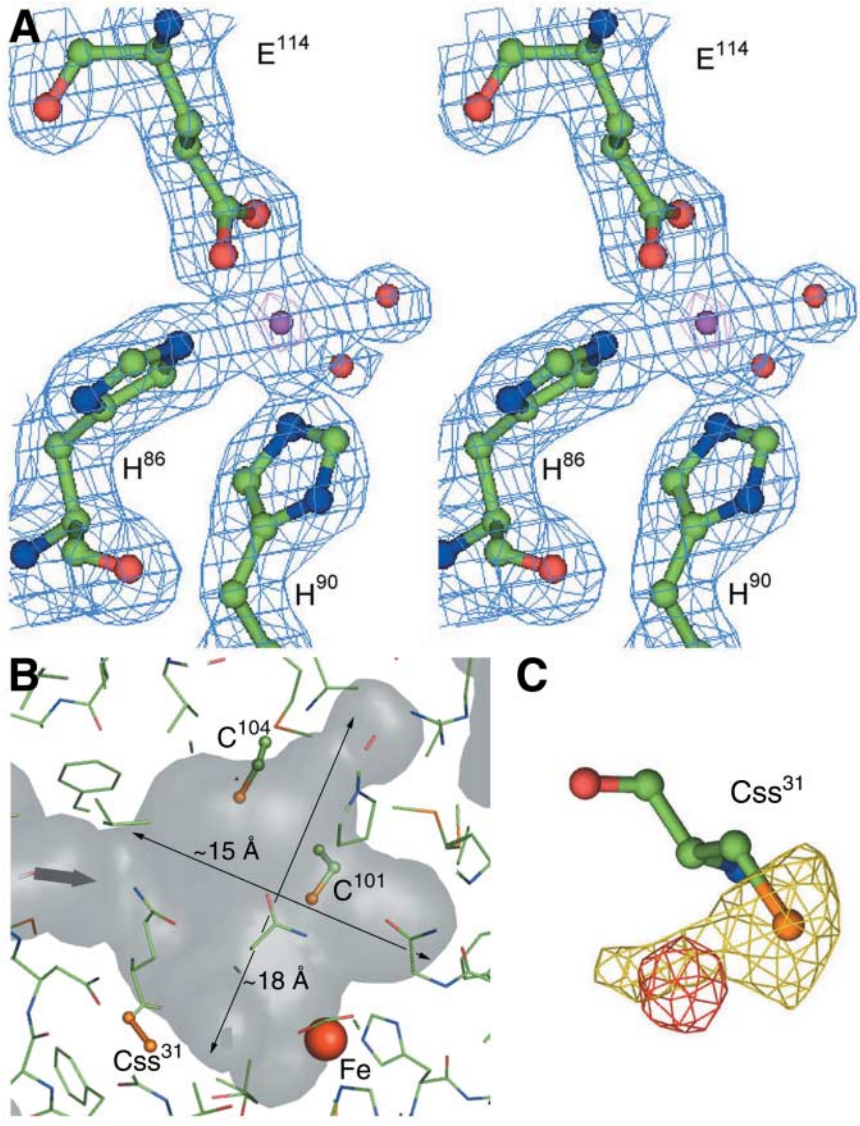

Fig. 3. The catalytic pocket containing the conserved cysteines and the iron. (**A**) Stereo view of the mononuclear nonheme iron center with Fe ligands, electron density contoured at 1 σ; purple sphere, Fe ion; red, waters; ball-and-stick, protein ligands. (**B**) Cavity surface representation of the catalytic pocket with Cys and Fe highlighted; gray arrow, cavity entrance. (**C**) Identification of an additional sulfur atom at Cys31. The position of the additional atom is indicated by the red mesh blob in a six-fold averaged difference Fourier (m|Fo| − D|Fc|) map contoured at 5 σ. The sulfur nature of the additional atom was confirmed by the six-fold averaged anomalous difference map in yellow mesh, calculated using the iron κ-edge data contoured at 3 σ.

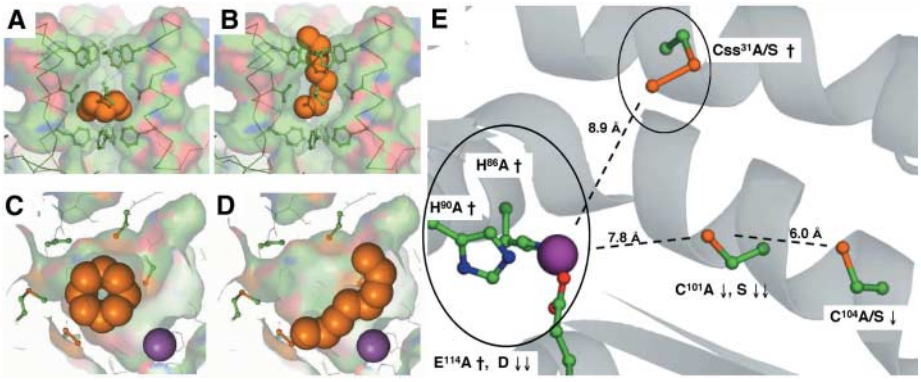

Fig. 4. Substrate access and essential residues for enzyme activity. (**A** and **B**) In silico modeling of α-S_8 sulfur and linear polysulfide, respectively, represented by Van der Waals spheres into the four-helix bundle chimneys, which lead to the interior of the sphere; gatekeeping residues in ball-and-stick representation. (**C** and **D**) α-S_8 sulfur and linear polysulfide modeled as putative substrates at the catalytic pocket, with Fe represented as a purple sphere and catalytic cysteines in ball-and-stick representation; inner surface of catalytic pocket in transparent color. (**E**) Effect of mutants on SOR activity (*23*). The core active site composed of the Fe site and the persulfide-modified Css31 is highlighted within ellipsoids. †, zero activity; ↓, reduced activity; ↓↓, strongly reduced activity.

Cys104 reside in the same helix (Fig. 4E), with their sulfur atoms 6.0 Å apart, too distant to allow disulfide bridge formation even when assuming alternate side-chain conformations. Consequently, no second redox-active site is seen in the SOR, which could assist in performing the rather complex sulfur disproportionation chemistry. The final difference Fourier maps consistently revealed an electron density blob at ~3 to 5 σ at 2.2 Å from Sγ of the essential Cys31 in all six monomers of the asymmetric unit, indicating the presence of an additional atom (Fig. 3C). Averaged anomalous difference Fourier maps using the iron κ-edge wavelength data also showed anomalous scattering at that site, and Cys31 was refined as cysteine persulfide (Css). The terminal sulfane S_δ is oriented toward the iron site, at a distance of 8.9 Å (Fig. 4E). Sulfane sulfur atoms are reactive labile species (*28*), which are generated in the catalytic cycles of various enzymes acting as sulfur transferases in the biosynthesis of sulfur-containing biomolecules (*21*, *29*), but also in enzymes of the sulfur cycle, such as the oxidative thiosulfate transferase from the Sox complex of bacteria (SoxAX) (*30*, *31*) and the polysulfide-binding Sud protein from *Wolinella succinogenes* (*32*). The persulfurated cysteine is the covalent binding site of the substrate in all of these enzymes, indicating that this is also the function of Css31 in SOR, in accordance with mutagenesis studies (*23*, *24*).

The presence of the Css modification in the recombinant SOR crystal structure is remarkable, because the enzyme has not undergone catalytic turnover, and indicates that persulfuration is established before catalysis. There is accumulating evidence that Css are indeed catalytically active species and not intermediates. The recombinant SoxAX protein was described as persulfurated in the absence of its substrate thiosulfate (*31*). This was also observed in a sulfur transferase from *Azotobacter vinelandii* (*29*). Formation and use of Css may thus be a widespread mechanism in inorganic sulfur biochemistry.

To date, five other SOR proteins or genes are known showing 39% to 88% sequence identity with *A. ambivalens* SOR (fig. S1A), and they likely have a similar three-dimensional fold. Highly conserved regions can be identified when plotting the 77 amino acids onto the monomer structure, which are identical in the available sequences (25% of the *A. ambivalens* SOR) (fig. S3E). Notably, 19 out of 23 (83%) residues in an 8 Å radius around the Fe ion are conserved in all SOR sequences, highlighting the functional relevance of the iron site and its primary and secondary ligand sphere. In addition, 21 out of 38 residues (55%) lining the catalytic pocket are conserved, showing the conservation of functionally important residues during evolution and corroborating our identification of the catalytic pocket.

The architecture of the SOR suggests the enzyme's mode of action. Because the 24 active sites are not directly accessible from the exterior, sulfur must enter the sphere before catalysis. Thus, the SOR creates a reaction chamber separated from the cytoplasmic environment. The six chimney-like protrusions are the likely entry routes. These are characterized by a hydrophobic, apolar inner surface (Fig. 4, A and B). Functionally, they can be interpreted as filters for the selection of the correct substrate. The substrate is then delivered to one of the 24 active sites. It has not been determined whether the substrate of the SOR is cyclic α-S_8 or a linear, more soluble sulfur species, such as a polysulfide. In silico modeling showed that α-S_8 is too bulky to travel across the accessing chimney-like pores or to cross the entrance to the active-site pocket without considerable structural rearrangements, whereas linear polysulfides could more easily pass, which indicates that sulfur is linearized (Fig. 4, A to D, and movie S2). In addition, the positive charge of the inner surface might favor the negatively charged anions over the hydrophobic elemental sulfur. After entering the active-site pocket, the substrate is covalently bound to Css31, which is probably in the negatively charged persulfide state. Upon binding, the substrate gets aligned close to the Fe site (movie S2), which, in mechanistic analogy to other 2-His-1-carboxylate facial triad enzymes, probably results in the displacement of one or both water ligands, leading to a coordinatively unsaturated pentacoordinated Fe site that would be poised to bind dioxygen (*25*, *33*). At that stage, the center is probably in the Fe^{II} state, eventually by a one-electron transfer from the cysteine-bound polysulfide. This would also allow oxygen binding to give a peroxo species as the first intermediate. Interestingly, the low reduction potential of the iron site (E_m = –268 mV) (*12*) is in the range of the H_2S/S^0 couple (E_0' = –270 mV) (*34*), suggesting that this is also the site of sulfur reduction. Because the two other cysteine residues are not essential for catalysis, as shown by site-directed mutagenesis (*23*), Css31 and the iron constitute the enzyme's core active site (Fig. 4E). The fate of the reaction products and their pathway upon leaving the SOR sphere has not been resolved.

The structural similarity between the SOR and ferritins and the presence of related active sites in which the confined substrates react with molecular oxygen suggest that these proteins are an example of structural and, to some extent, functional convergent evolution. In addition, our results show how prokaryotes circumvent the lack of compartmentation within their cytoplasm by generating proteinaceous nanocompartments through the oligomerization of proteins.

References and Notes

1. D. P. Kelly, *Phil. Trans. R. Soc. Lond. Ser. B* **298**, 499 (1982).
2. D. P. Kelly, J. K. Shergill, W. P. Lu, A. P. Wood, *Antonie Van Leeuwenhoek* **71**, 95 (1997).
3. G. J. Olson, J. A. Brierley, C. L. Brierley, *Appl. Microbiol. Biotechnol.* **63**, 249 (2003).
4. P. Schönheit, T. Schäfer, *World J. Microbiol. Biotechnol.* **11**, 26 (1995).
5. C. G. Friedrich, D. Rother, F. Bardischewsky, A. Quentmeier, J. Fischer, *Appl. Environ. Microbiol.* **67**, 2873 (2001).
6. C. G. Friedrich, F. Bardischewsky, D. Rother, A. Quentmeier, J. Fischer, *Curr. Opin. Microbiol.* **8**, 253 (2005).
7. J. Boulegue, *Phosphorus Sulfur* **5**, 127 (1978).
8. A. Kletzin, *J. Bacteriol.* **171**, 1638 (1989).
9. A. Kletzin, T. Urich, F. Müller, T. M. Bandeiras, C. M. Gomes, *J. Bioenerg. Biomembr.* **36**, 77 (2004).
10. T. Emmel, W. Sand, W. A. König, E. Bock, *J. Gen. Microbiol.* **132**, 3415 (1986).
11. Z. He, Y. Li, P. Zhou, S. Liu, *FEMS Microbiol. Lett.* **193**, 217 (2000).
12. T. Urich *et al.*, *Biochem. J.* **381**, 137 (2004).
13. Materials, methods, and refinement statistics are available as supporting material on *Science* Online.
14. A. Kletzin, *J. Bacteriol.* **174**, 5854 (1992).
15. S. Macedo *et al.*, *Nat. Struct. Biol.* **10**, 285 (2003).
16. C. Zhang, S. H. Kim, *J. Mol. Biol.* **299**, 1075 (2000).

17. J. S. Richardson, *Adv. Protein Chem.* **34**, 167 (1981).
18. G. Sciara *et al.*, *EMBO J.* **22**, 205 (2003).
19. R. Wu *et al.*, *J. Biol. Chem.* **280**, 2840 (2005).
20. A. Ebihara *et al.*, *J. Struct. Funct. Genomics* **6**, 21 (2005).
21. J. H. Ploegman *et al.*, *Nature* **273**, 124 (1978).
22. D. Lang, R. Thoma, M. Henn-Sax, R. Sterner, M. Wilmanns, *Science* **289**, 1546 (2000).
23. T. Urich *et al.*, *FEMS Microbiol. Lett.* **248**, 171 (2005).
24. Z. W. Chen, C. Y. Jiang, Q. She, S. J. Liu, P. J. Zhou, *Appl. Environ. Microbiol.* **71**, 621 (2005).
25. M. Costas, M. P. Mehn, M. P. Jensen, L. Que Jr., *Chem. Rev.* **104**, 939 (2004).
26. A. Karlsson *et al.*, *Science* **299**, 1039 (2003).
27. O. A. Andersen, T. Flatmark, E. Hough, *J. Mol. Biol.* **320**, 1095 (2002).
28. H. Beinert, *Eur. J. Biochem.* **267**, 5657 (2000).
29. D. Bordo *et al.*, *J. Mol. Biol.* **298**, 691 (2000).
30. V. A. Bamford *et al.*, *EMBO J.* **21**, 5599 (2002).
31. U. Kappler, G. R. Hanson, A. Jones, A. G. McEwan, *FEBS Lett.* **579**, 2491 (2005).
32. Y. J. Lin *et al.*, *Biochemistry* **43**, 1418 (2004).
33. K. D. Koehntop, J. P. Emerson, L. Que Jr., *J. Biol. Inorg. Chem.* **10**, 87 (2005).
34. R. K. Thauer, K. Jungermann, K. Decker, *Bacteriol. Rev.* **41**, 100 (1977).
35. The authors wish to thank F. Pfeifer (Darmstadt), M. Teixeira and M. A. Carrondo (both Oeiras) for encouragement and support, T. M. Bandeiras for valuable experimental assistance, and the staff at European Synchrotron Radiation Facility Grenoble (France) and European Molecular Biology Laboratory, Outstation Hamburg (Germany). This work was supported by a grant from the Deutsche Forschungsgemeinschaft (to A.K., Kl885/3-3) and by a Deutscher Akademischer Austausch Dienst (Germany) and Gabinete de Relações Internacionais da Ciência e do Ensino Superior (Ministério da Ciência, Inovação e Ensino Superior, Portugal) collaborative travel grant (to A.K. and C.M.G.). T.U. was awarded a Marie Curie fellowship for the structure determination at Instituto Tecnologia Química e Biológica (Oeiras). The atomic coordinates of the SOR have been deposited in the Protein Data Bank at www.rcsb.org (accession code 2CB2).

Supporting Online Material

www.sciencemag.org/cgi/content/full/311/5763/996/DC1
Materials and Methods
Figs. S1 to S4
Tables S1 and S2
References and Notes
Movies S1 and S2

19 September 2005; accepted 13 January 2006
10.1126/science.1120306

A Keystone Mutualism Drives Pattern in a Power Function

John Vandermeer[1,2]* and Ivette Perfecto[2]

Data that can be described by a power function are ubiquitous in nature. Although there is consensus that such data frequently emerge generally from nonlinear complex systems, a variety of specific mechanisms may be responsible for creating the pattern in particular cases. Here, we report on the distribution of a scale insect (*Coccus viridis*) that is a common agricultural pest. Its distribution in an organic coffee farm in southern Mexico generally follows a power function, but there are subtle deviations from that function. We offer a biological explanation for both adherence to the power functions and associated deviations, along with supporting evidence.

The distribution of clusters of organisms, much like other patterns in nature (*1*, *2*), is frequently characterized by a power function (*3*). For a variety of distinct dynamic scenarios, when cast in a spatial framework, biological interactions of several distinct types are capable of generating spatial pattern characterized by power law scaling (*4*). This pattern is usually interpreted as a signal of self-organization resulting from spatial extension. In most ecological examples, clusters are formed through various biological interactions manifest in a spatial context, such as local depletion of resources (*5*), local disturbance regimes (*6*) or predator-prey interactions (*7*). That clusters form in the first place is an interesting aspect of these theories, but the evidence that the distribution of individuals within those clusters approximates a power law is the most intriguing aspect of self-organization (*2*). Any spatial process that combines a local spread (for example, local production of a prey population) with a regional control (for example, a searching predator that ranges widely) will likely generate clusters (*8*). A similar mechanistic statement is more elusive for the power function nature of those clusters.

For the green coffee scale (*C. viridis*), the formation of clusters is of little interest because each "cluster" is a population of scale insects on a coffee bush. However, the ecology of this organism offers a potential explanation of both the evident power law and subtle deviations from it at high and low population sizes.

The green coffee scale is a common herbivore, frequently noted as a pest in greenhouses and a known pest of coffee (*9*, *10*). Although normally maintained by natural enemies below critical damage thresholds, it can sometimes reach pest status (*11*). It is tended by a variety of ant species in a classic mutualistic form: The homopteron supplies honeydew to the ant, and the ant protects the homopteron from predators (*12*). *Azteca instabilis*, a mutualist of *C. viridis* in southern Mexico (*13*), is a tree-nesting species that occurs in obvious spatial clusters (*14*) in the shade trees of coffee farms. Those coffee bushes that are near a tree occupied by *A. instabilis* are frequently sites of large concentrations of *C. viridis*. At least two species of encyrtid wasps are parasitoids on *C. viridis* and the coccinelid beetle *Azya orbigera* is a voracious predator. Direct observations and experimental results indicate that the *A. instabilis* ants are efficient protectors of the scale insects in the face of these natural enemies (*15*), and casual observations leave little doubt that the ants collect honeydew from the scales.

To investigate the spatial pattern of *C. viridis*, we set up a 45-ha plot on an organic coffee farm in southwestern Mexico (*16*), identified each shade tree therein, and assessed whether or not it contained an *A. instabilis* colony (*13*). Of 10,597 trees located, 276 contained *A. instabilis* colonies. We systematically chose five locations surrounding such a colony and four locations that were clearly outside of the influence of any such colony (*17*). In each of the nine sites, we determined the scale abundance (*17*) on approximately 50 to 100 coffee plants, for a total of 678 coffee plants surveyed.

The frequency distribution of scale insect numbers per tree is shown in Fig. 1. A power function is clearly suggested by the approximately linear nature of the points. However, subtle deviations from the power function at both high and low scale densities are also evident by casual observation. Because of the deviations at both high and low densities, we

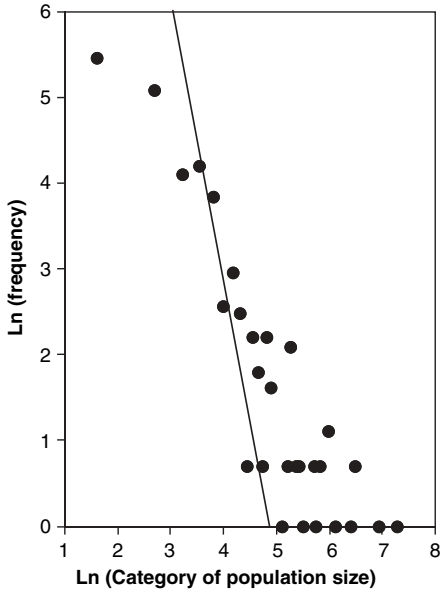

Fig. 1. Log-log plot of population size versus frequency of size of cluster. The line is a regression based on the data points located between 3.5 and 4.5 on the abscissa (*17*). Slope of power function is –2.72.

[1]Department of Ecology and Evolutionary Biology, [2]School of Natural Resources and Environment, University of Michigan, Ann Arbor, MI 48109, USA.

*To whom correspondence should be addressed. E-mail: jvander@umich.edu